https://doi.org/10.22226/2410-3535-2022-4-336-342

Structure and electrical potential of calcium phosphate coatings modified with aluminum oxyhydroxide nanoparticles

V. V. Chebodaeva[†,1,2], M. B. Sedelnikova[1], A. D. Kashin[1], O. V. Bakina[1], I. A. Khlusov[2], A. L. Zharin[3], V. S. Egorkin[4], I. E. Vyaliy[4], Yu. P. Sharkeev[1]

[†]vtina5@mail.ru

[1]Institute of Strength Physics and Materials Science, RAS, Tomsk, 634055, Russia
[2]Siberian State Medical University, Tomsk, 634050, Russia
[3]Belarusian National Technical University, Minsk, 220013, Belarus
[4]Institute of Chemistry, Far Eastern Branch of the RAS, Vladivostok, 690022, Russia

The effect of the introduction of charged aluminum oxyhydroxide (AO) nanoparticles into the porous coatings from calcium phosphate formed by micro-arc oxidation on their electrical potential and structure was studied. The modification resulted in changes in the morphology and elemental composition of the coatings. The selection of coating functionalization parameters resulted in obtaining homogeneously distributed aluminum oxyhydroxide nanoparticles in the form of agglomerates, providing the maximum change in the electrical potential of the coatings. An increase in the duration of ultrasonic dispersion (USD) of initial AlN powder suspension from 10 to 60 min and an increase in the surface roughness of the coatings, parameter R_a, from 3.5 to 5.5 μm led to an increase in the surface electrical potential from −85 to −35 mV. At the same time, the aluminum content in the coating decreased from 3 to 1 at.% with an increase in the duration of USD of the AlN powder suspension from 10 to 60 minutes. The introduction of aluminum oxyhydroxide nanoparticles into the coating contributed to an improvement in corrosion properties, namely, an increase in the corrosion potential from 0.1 to 0.2 mV and a decrease in the corrosion current from $2.5 \cdot 10^{-9}$ to $1.1 \cdot 10^{-9}$ A · cm^2.

Keywords: electrical potential, calcium phosphate coatings, micro-arc oxidation, implants, titanium.

1. Introduction

Metal implants for osseointegration have been successfully used in orthopedic surgery for several decades. However, in 15% of surgical cases implants are not integrated into the surrounding bone tissue [1–4]. In most cases, titanium and titanium-based alloys are used to manufacture bone implants. This is due to their mechanical properties, high strength, biocompatibility and high corrosion resistance [1–4,7]. Magnesium and zirconium alloys have also recently been used as materials for implants [3,8–11].

The interaction between the implant materials and the biological medium occurs at the phase interface, therefore properties such as chemical composition, surface energy, roughness and topography are very important [7,12–19]. Rough and porous surfaces have a more pronounced and positive effect on the cell activity than smooth ones. Researchers often apply bioactive coatings to create the desired chemical composition and roughness of the implant surface. In addition to the topography of the surface, the cell adhesion is affected by the surface charge of the implant. It is evident from the experimental data [7,10–13] that the charged surface of hydroxyapatite (HA) ceramics increases osteoconductivity and promotes bone tissue regeneration.

The Micro Arc Oxidation (MAO), also known as Plasma Electrolytic Oxidation (PEO) [8–11], is often used to form calcium phosphate (CP) coatings on the surface of metals such as Ti, Al, Mg, Zr and their alloys to improve their bioactivity and corrosion resistance. In addition, the biocoatings formed by this method have high porosity, which enables them to be saturated with various antibacterial agents [7,12–13,8–11].

Modification of porous coatings is a promising direction in biomedical materials science. For instance, the authors of [7,8–11,13] introduce nanoparticles, halloysite nanotubes, polymer or β-tricalcium phosphate (β-TCP) particles into the electrolyte composition to improve the functional properties of the coatings such as mechanical strength and corrosion resistance. In addition, coatings are often modified with polymers to protect against corrosion processes [9,11].

Intensive research has been conducted to develop systems based on inorganic two-dimensional nanostructures with controlled drug delivery. Nanoparticles have a high value of specific surface energy due to their small size, which ensures their high chemical activity [20–22]. It is known that nanostructured aluminum oxyhydroxide (AO) is used as a sorbent in the manufacture of microbiological filters and antiseptic dressings due to its antibacterial properties [20,21]. AO nanoparticles obtained by the electric explosion method carry an electropositive charge after interaction with aqueous media, which allows them to be used to change the electrical potential of the surface of biological coatings [7,20]. It is evident that the introduction of such nanoparticles into a CP coating

will change its charge state and antibacterial characteristics. Modification of biomaterials with such nanoparticles will improve their bioactive and chemical properties.

Thus, the aim of the work is the modification of CP coatings in order to change the electrical and structure of coatings.

2. Materials and experimental methods

Titanium samples with the dimensions of (10×10×1 mm^2) were cut from commercially pure titanium (Grade 2) and subsequently sanded using 320- and 600-grit waterproof abrasive paper to remove natural surface oxide.

The samples were then ultrasonically cleaned in ethanol and distilled water [7,13]. The electrolyte contained an aqueous solution of orthophosphoric acid (solution of H_3PO_4), calcium carbonate ($CaCO_3$), and mechanochemically synthesized HA ($Ca_{10}(PO_4)_6(OH)_2$) [23]. CP coatings were applied anodically with the following MAO parameters: processing voltage of 200 V, pulse duration of 100 μs, pulse repetition rate of 50 Hz, coating deposition duration of 10 min. The electrolyte temperature was maintained below 30°C. The resulting porous coatings were functionalized with AO nanoparticles obtained by hydrolysis of 30 mg of AlN powder in 25 ml of distilled water. AlN nanoparticles were obtained by the method of electrical explosion of Al wire in a nitrogen atmosphere, as described earlier [7,20]. AO nanoparticles were deposited on the CP coatings using hydrolysis reaction, as described previously [7], with preliminary ultrasonic dispersion (USD) of AlN powder suspension.

The morphology of the samples was studied by scanning electron microscopy (SEM) on a LEO EVO 50 electron microscope (Carl Zeiss, Germany) equipped with an INCA-Energy 350 EDS analyzer (Oxford Instruments, Abingdon, UK). The X-ray analysis of titanium plates with CP coatings was carried out on a DRON-7 diffractometer (Burevestnik, Russia) with Bragg-Brentano geometry and Co-K_α radiation ($\lambda = 0.17902$ nm) at 2θ angles in the range of 10 – 90°, a scanning angle step of 0.03° and an exposure time of 9 s. Both of these studies were carried out at the ISPMS SB RAS' Center for Collective Usage "Nanotech" (Tomsk, Russia). The surface roughness was estimated as average roughness (R_a) using a Hommel-Etamic T1000 profilometer (Jenoptic, Jena, Germany) at the Tomsk Polytechnic University.

The electrical potential (EP) was measured using the contact potential difference (CPD) method. The non-vibrating CPD method based on the Kelvin scanning probe method was implemented on a specialized scanning unit (Belarusian National Technical University (Minsk, Belarus)) to measure the electrical properties of CP coatings [24,25]. For evaluation of the corrosion behavior of the CP coatings on titanium substrates Versa STAT MC system (Princeton Applied Research, Oak Ridge, TN, USA) was used. Measurements were carried out in a three-electrode cell K0235 with Ringer solution used as an electrolyte at the temperature of 37°C.

3. Results and discussion

Figure 1 shows the surface of CP coatings before and after modification by AO nanoparticles and Al map distribution on CP coating surface. The unmodified coating is represented by numerous spheroidal formations with pores. This morphology is characteristic of coatings obtained by the MAO method and is due to the processes occurring in the electrolyte [7,13,18,28]. The Table 1 shows the elemental composition of CP coatings. The main elements contained in the coating are

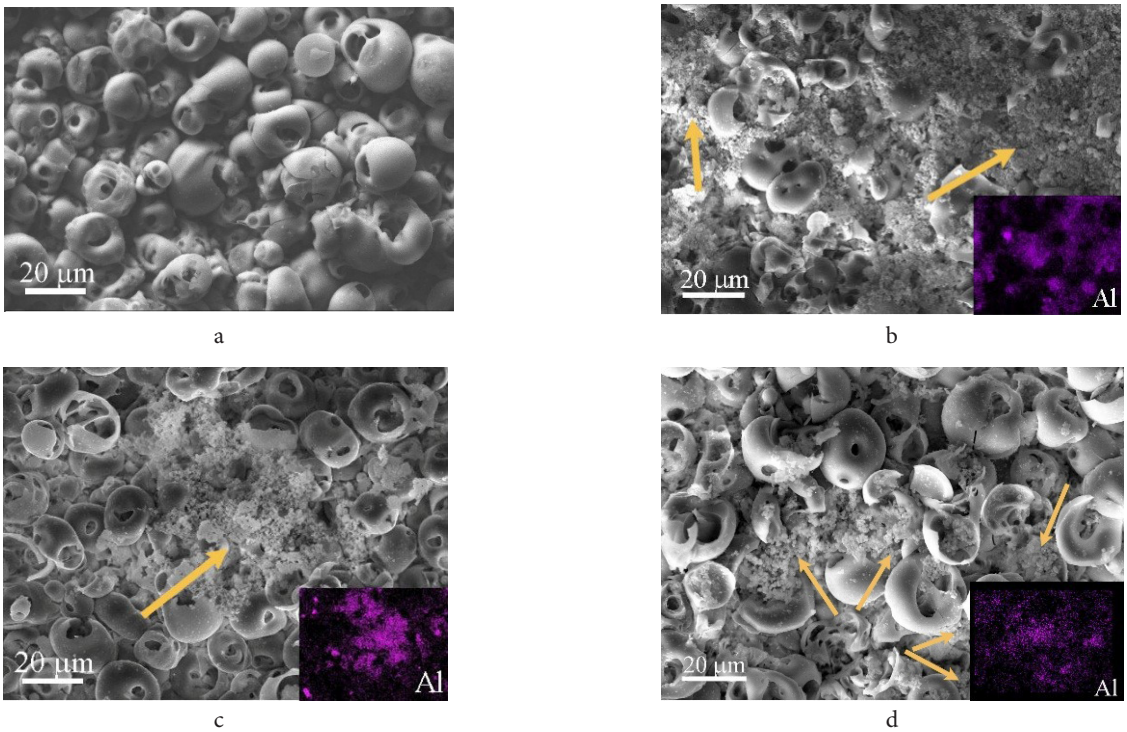

Fig. 1. (Color online) SEM images of CP coatings formed at a MAO voltage of 200 V (a) and Al map distribution of CP coatings functionalized by AO nanoparticles after various duration of USD of AlN suspension, min: 20 (b), 40 (c), 60 (d); arrows point to the agglomerates of AO nanoparticles.

Ca and P (Table 1). The roughness R_a of such coatings was 3.3 μm. After the introduction of AO nanoparticles, dense agglomerates of the AO nanoparticles appeared on the coating surface as a result of 20 min of USD (Fig. 1b). The Al content in such coatings was 3 at.% (Table 1). The roughness of the coatings after the introduction of nanoparticles increased to 3.5 μm. The subsequent increase in the duration of USD of the AlN suspension led to a more uniform distribution of AO nanoparticles over the coating surface and a decrease in the Al content to 1 at.% (Table 1). As a result of increasing the duration of USD of suspensions with AlN powder, the structural elements of the coating partially collapsed. This and the presence of AO nanoparticles in the coating led to an increase in the roughness of the coatings from 3.5 to 5.5 μm after an increase in the USD duration from 10 to 60 min.

Figure 2 shows the images of the coating cross-section with the distribution of elements along its thickness. It can be seen that CP coatings have a pore structure with an average pore size of 4 μm and are characterized by both closed and open through pores [7,18]. The analysis of the elemental composition in the cross-sections of coatings (Fig. 2) showed that the distribution of the main elements (Ca and P) is homogeneous. It can also be seen that the amount of Ti is high, and its concentration increases near the substrate. In the coating modified with AO nanoparticles, it can be seen that the amount of Al increased in the pores of the coatings. This confirms the presence of AO nanoparticles within the inner volume of the coating, which provides their gradual release during the dissolution of the coating in a human physiological medium. The small size of the nanoparticles of the initial AlN powder (≈90 nm) [21,22] allows their penetration into the interstitial spaces and pores of the CP coating. After hydrolysis of AlN [7,21,22] the AO nanoparticles of an average size of ≈100–250 nm were formed. An increase in the size of the formed nanoparticles allows "fixation" in the coating pore and, as a result, the release of these nanoparticles into the environment becomes difficult.

Table 1. Elemental composition of CP coatings.

Element/ USD, min	At.%					
	0	20	30	40	50	60
Al	-	3	2	1	1	1
O	71	68	69	69	69	70
P	14	13	13	15	14	14
Ca	3	4	4	3	4	3
Ti	12	12	12	12	12	12

Previous studies have shown that such coatings have an antibacterial effect [7]. Many works are devoted to the modification of porous materials [7,13,25,26] confirm the positive effect of the gradual release of antibacterial additives. This allows for a longer antiseptic effect on bacteria and prevents possible complications in case of infection in the implantation area.

The results of the X-ray phase analysis showed that the coatings are X-ray amorphous. This is confirmed by the presence of diffuse scattering regions on all diffractograms (Fig. 3). Peaks from the substrate material — Ti are present on the diffractograms. This method of studying the phase composition of the coating did not reveal the presence of Al compounds due to its low content. As can be seen in [7] AO nanoparticles are weakly crystallized and are represented by the pseudoboehmite phase. Unlike crystalline boehmite, for pseudoboehmite, there is a decrease in the main maxima and a broadening of the peaks. This is due to the content of more water ($Al_2O_3 \cdot 1.4\,H_2O$) compared to the stoichiometry of boehmite. Additional water molecules cannot be located in the interlayer space without disturbing the regular structure of AlO(OH). This leads to a violation of the coherence of the scattering of two adjacent layers. The obtained results are consistent with the elemental analysis data, which showed that the Al content in the coatings does not exceed 1–3 at.% (Table 1).

Figure 4 illustrates the 3D and 2D images of the electrical potential distribution on the surface of MAO coating surface without modifications (Fig. 4a,b) and after different durations of USD of the AlN nanoparticles (Fig. 4c–h). Examination of the charge distribution using the non-vibrating CPD

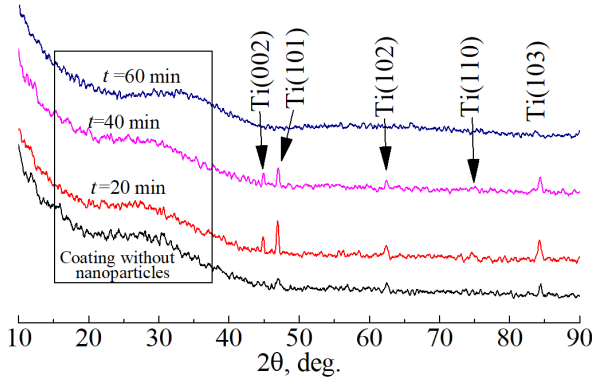

Fig. 3. (Color online) XRD patterns of the control and CP coatings with AO nanoparticles after different durations of USD (the rectangle highlights the diffuse scattering regions).

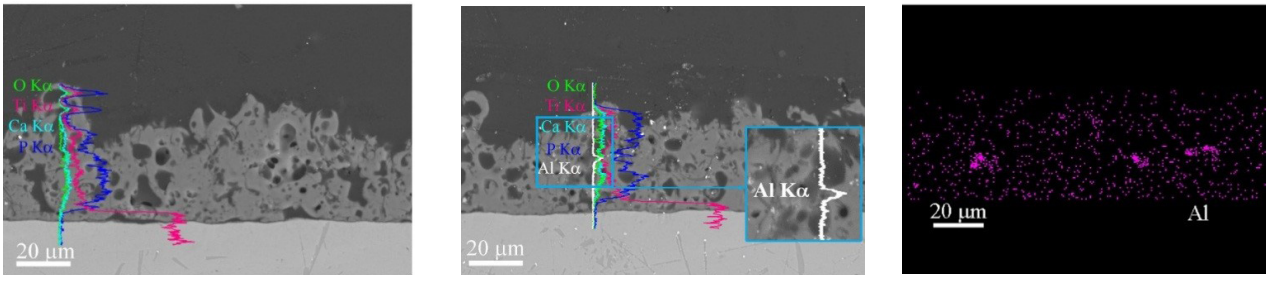

a b c

Fig. 2. (Color online) Element distribution line scan (a, b) and map of Al distribution (c) in the cross-section of the CP coatings (a) and coatings functionalized by AO nanoparticles after USD of AlN suspension for 60 min (b, c).

method showed that all coatings had a negative surface potential which ranged from −107 to −35 mV (Fig. 4, Fig. 5). The negative potential of the coating surface is conditioned by the formation of the coating in the anodic mode. In this mode, the titanium sample acts as an anode and a positive potential applied to it. This causes ions of the opposite sign, negative, to flow onto the sample. Other works confirm this regularity [7, 26, 28, 29]. The 3D visual representation of the electrical potential distribution is given to estimate the magnitude of the deviation of the electrical potential of the

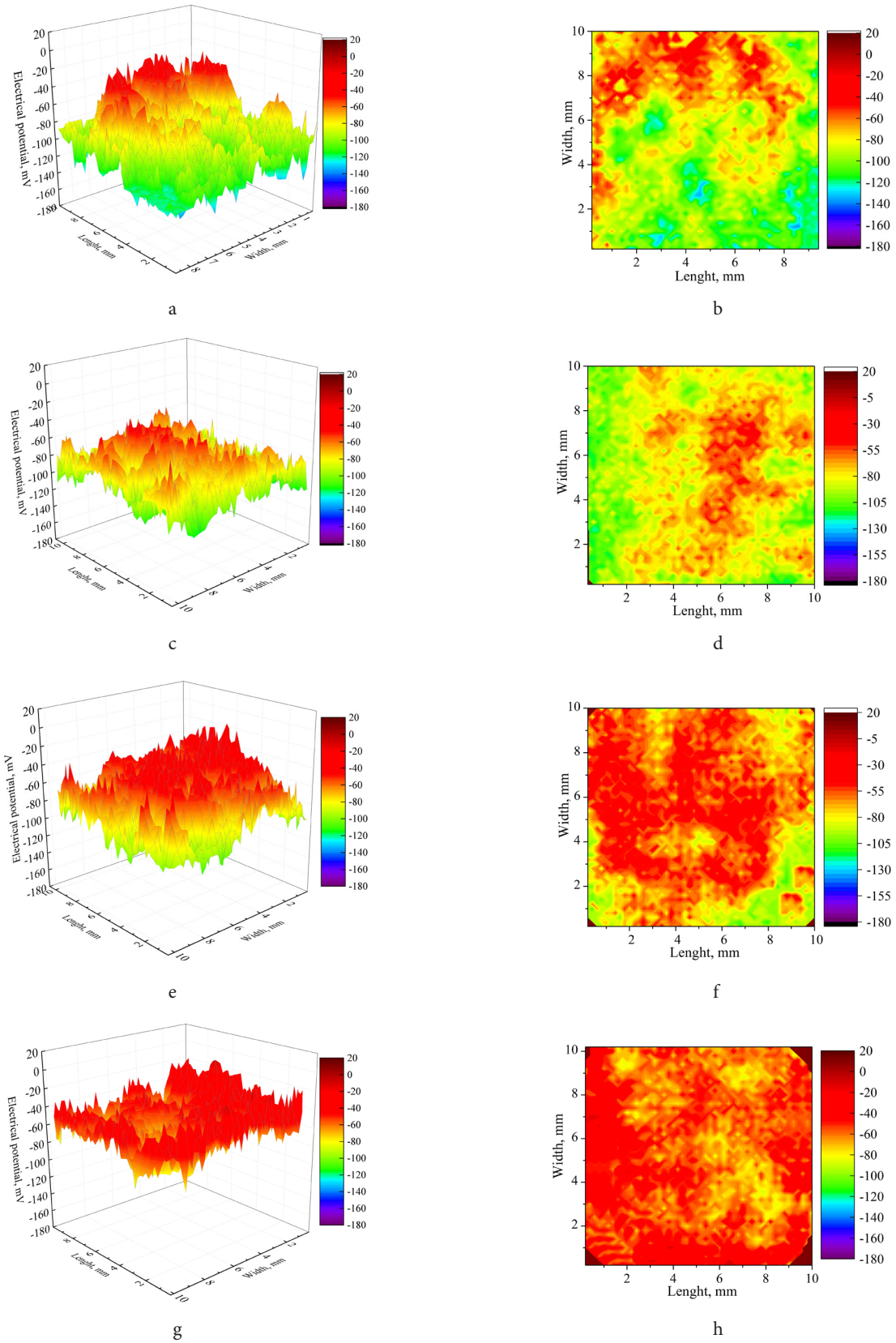

Fig. 4. (Color online) 3D (a, c, e, g) and 2D (b, d, f, h) images of the electrical potential distribution on the surface of MAO coatings without AO nanoparticles (a, b) and after different durations of USD, min: 20 (c, d), 40 (e, f), 60 (g, h).

coating. Meanwhile, the 2D format of displaying the potential distribution makes it possible to estimate the uniformity of the distribution and the magnitude of the electrical potential of the coatings. It can be seen that the charge was distributed inhomogeneously over the surface of the control CP coating, the average value was −85 mV (Fig. 4 a, b, Fig. 5).

On the surface of the 3D charge distribution of the coating, several peaks can be observed on one half of the sample surface with a value of up to −20 mV. The presence of local extremes can be explained by the clusters of defects or heterogeneity of processes occurring during the formation of coatings by the MAO method [7,13,18]. However, both the surface and its volume are used in the measurements of the electrical potential by this method. Therefore, determining the type and depth of the defect is a challenging task [27, 26].

As can be seen from Fig. 5, modification by nanoparticles after 10 minutes of USD leads to a decrease in the average charge value to −107 mV. An increase in the duration of USD to 20 min led to a more homogeneous distribution of the charge over the coating surface, which can be seen in the 2D image of the potential distribution (Fig. 4 d). The intensity of the maximum deviations in the magnitude of the potential decreased after the introduction of AO nanoparticles (Fig. 5 c, d). This can be attributed to the appearance of large agglomerates of AO particles in the coating and increased uneven charge distribution. The average value of the electrical potential increased to −82 mV (Fig. 5). Figures 4 e – h demonstrate an increase in the magnitude of the electrical potential of the coatings in the electropositive region. The average values of electrical potentials increased to −50 and −35 mV, respectively. These results correlate with the dependence of the roughness parameter R_a on the USD duration. It can be seen that increasing the roughness from 3.5 to 5.5 μm increases the electrical potential of the coatings from −85 to −35 mV. The paper [31] provides information on the dependence of the magnitude of the electrical potential of coatings on the features of its topography. The presence of peaks on the sample surface leads to an increase in the electrical potential of the coatings measured by the Kelvin scanning probe method [31]. In addition, other works also confirm the dependence of the electrical properties of the surface of materials on their roughness [7, 29 – 31].

The most homogeneous distribution of the surface potential among the group of samples containing AO nanoparticles has the coating modified after 60 minutes of dispersion (Fig. 4 g, h). The presence of homogeneously distributed positively charged AO nanoparticles resulted in the highest value of the electrical potential among all samples (Fig. 5). A decrease in the values of the surface charge in certain areas indicates a lower density of filling of the surface states associated with the partial destruction of the elements of the coating structure as a result of ultrasonic exposure.

Figure 6 illustrates the linear dependence of the average CP coating charge on the duration of suspension dispersion. The average charge value of the control coating was equal to −85 mV. The shift of the electrical potential of the coating to the positive region is due to the compensation of the negative potential of coatings by nanoparticles having a positive surface potential.

An increase in the USD duration from 10 to 60 minutes leads to a linear increase in the average value of the potential from −107 to −35 mV. It can be seen from the 3D distributions that the values of the electrical potential are distributed more homogeneously over the surface compared to coatings before modification by AO nanoparticles. Thus, the study of the electrical characteristics of coatings by the non-vibrating CPD method confirms the influence of these nanoparticles on the magnitude and distribution of the electrical potential of the coating.

Figure 6 shows the polarization curves and Fig. S1 (supplementary material) shows the evolution of the open circuit potential for titanium samples with CP coatings without AO nanoparticles and for samples with CP coatings modified with AO nanoparticles after USD of AlN suspension for 60 min. Figure S2 (supplementary material) illustrates the Nyquist plot, equivalent electrical circuit used to calculate the impedance data and Bode plots of MAO coating surface without modifications and after 60 min of USD of the AlN nanopowder.

From the results of the study of the corrosion properties of the coatings, it follows that the coatings of both types are represented by a developed surface topography. At the same time, the impedance modulus for samples with CP coating modified with AO nanoparticles is $9.3 \cdot 10^6$ Ω·cm^2, which

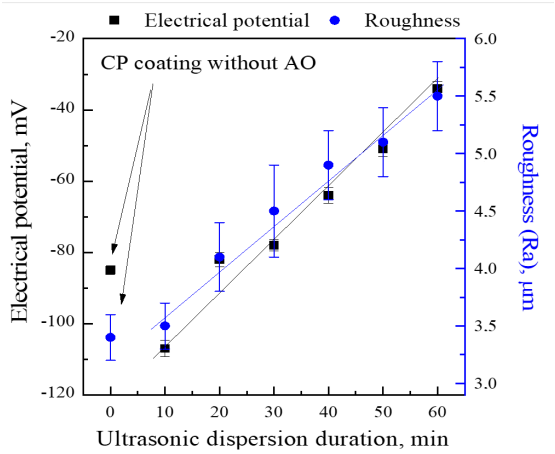

Fig. 5. (Color online) Electrical potential and roughness of the control and MAO coatings with AO nanoparticles after different durations of USD.

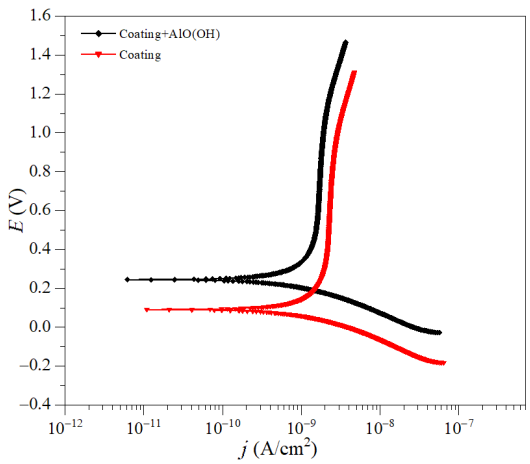

Fig. 6. (Color online) Potentiodynamic polarization curves obtained in Ringer solution.

Table 2. Electrochemical parameters of the samples.

Samples	E_C(V), mV	b_a (mV/decade)	$-b_c$ (mV/decade)	j_C, A·cm^2	R_p, Ω·cm^2	$\|Z\|$, Ω·cm^2
CP coatings +AlO(OH)	0.2	839	142	$1.1\cdot10^{-9}$	$1.6\cdot10^{7}$	$9.3\cdot10^{6}$
CP coatings	0.1	827	172	$2.5\cdot10^{-9}$	$2.4\cdot10^{6}$	$3.7\cdot10^{6}$

exceeds the value of the impedance modulus for samples without modifications almost twofold (Fig. 6, Table 2). The introduction of AO nanoparticles into the coating leads to an increase increase in the corrosion potential (E(V)) from 0.1 to 0.2 mV (Fig. 6, Table 2). An increase in the impedance modulus of the coatings indicates a decrease in the electrochemical activity of the sample. The presence of two-time constants (two bends in the graph of the phase angle (θ) versus frequency (Fig. S1b, supplementary material) indicates the presence of two layers, the lower nonporous layer and the upper porous layer.

Titanium samples with unmodified CP coatings are characterized by the highest values of the corrosion current density (j_C) of $2.5\cdot10^{-9}$ A·cm^2 and the lowest polarization resistance values (R_p) of $2.4\cdot10^{6}$ Ω·cm^2 (Table 2). After the introduction of AO nanoparticles into the CP coating, the corrosion current density decreases to $1.1\cdot10^{-9}$ A·cm^2, and the resistivity increases to $1.6\cdot10^{7}$ Ω·cm^2. This indicates an increase in the corrosion resistance of coatings as a result of their modification by AO nanoparticles.

In addition, the introduction of AO nanoparticles into the coatings leads to an increase in the corrosion potential and impedance modulus ($|Z|$) of the CP-coated samples to 0.2 mV and $9.3\cdot10^{6}$ Ω·cm^2, respectively (Table 2). The improvement of the protective properties of the modified coatings is due to the filling of the coating pores with AO nanoparticles and the change in the chemical composition of the coatings.

4. Conclusions

Bioactive calcium phosphate coatings with AO nanoparticles were formed by the micro-arc oxidation method. Calcium phosphate coatings were modified with AO nanoparticles after preliminary ultrasonic dispersion of AlN powder suspensions for 10 – 60 min. The obtained coatings were in an X-ray amorphous state, which was confirmed by the presence of diffuse scattering regions on the X-rays. Elemental analysis studies of cross-sectional fractures revealed that nanoparticles have penetrated into the inner pores of the coating. The roughness, parameter R_a, of the coatings as a result of modification by AO nanoparticles increased linearly from 3.5 to 5.5 μm.

The electrical potential of the coating modified with AO nanoparticles increased linearly with an increase in the duration of dispersion of the AlN suspension from 10 to 60 minutes and the roughness of the coating surface from 3.5 to 5.5 μm. As a result of the introduction of AO nanoparticles, the average electric potential increased linearly from −85 to −35 mV. Thus, AO nanoparticles in the coating have been shown to effect on surface charge, structure and other properties of the coatings. Modification of the coatings with the introduction of AO nanoparticles allowed to improve their corrosion resistance. This is evidenced by an increase in the corrosion potential and resistance from 0.1 to 0.2 mV and from $2.4\cdot10^{7}$ Ω·cm^2 to $1.6\cdot10^{6}$ Ω·cm^2, respectively. Moreover, the functionalization of coatings with AO nanoparticles contributed to a decrease in the corrosion current density from $2.5\cdot10^{-9}$ to $1.1\cdot10^{-9}$ A·cm^2. The developed approach of functionalization of CP coatings is a promising way to obtain materials with high bioactive properties.

Supplementary material. *The online version of this paper contains supplementary material available free of charge at the journal's Web site (lettersonmaterials.com).*

Acknowledgements. The work was performed according to the Government research assignment for ISPMS SB RAS, project FWRW-2021-0007 and was supported in part by Siberian State Medical University development program Priority 2030. The authors express their appreciation for the valuable contribution and assistance of Dr. M. A. Khimich (ISPMS, Tomsk, Russia).

References

1. N.E. Putra, M.J. Mirzaali, I. Apachitei, J. Zhou, A.A. Zadpoor. Acta Biomater. 109, 1 (2020). Crossref
2. A. Revathi, A.D. Borrás, A.I. Muñoz, C. Richard, G. Manivasagam. Mater. Sci. Eng. 76, 1354 (2017). Crossref
3. L. Li, M. Zhang, Y. Li, J. Zhao, L. Qin, Y. Lai. Biomater. 4 (2), 129 (2017). Crossref
4. B. Sharma, K. Nagano, M. Kawabata, K. Ameyama. Lett. Mater. 9 (4s), 511 (2019). Crossref
5. A.V. Lyasnikova, O.A. Dudareva, I.P. Grishina, O.A. Markelova, V.N. Lyasnikov. Lett. Mater. 8 (2), 202 (2018). (in Russian) Crossref
6. A.P. Rubshtein, A.B. Vladimirov, S.A. Plotnikov, V.B. Vykhodets, T.E. Kurennykh. Lett. Mater. 12 (2), 121 (2022). Crossref
7. V.V. Chebodaeva, M.B. Sedelnikova, O.V. Bakina, A.A. Miller, M.A. Khimich, K.S. Golohvast, A.M. Zaharenko, Yu.P. Sharkeev. Surf. Interfaces. 31, 101996 (2022). Crossref
8. B. Mingo, Y. Guo, A. Nemcova, A. Gholinia, M. Mohedano, M. Sun, A. Matthews, A. Yerokhin. Electrochim. Acta. 299, 772 (2019). Crossref
9. A.S. Gnedenkov, S.V. Lamaka, S.L. Sinebryukhov, D.V. Mashtalyar et al. Corros. Sci. 182, 109254 (2021). Crossref
10. M. Sun, A. Yerokhin, M.Ya. Bychkova, D.V. Shtansky, E.A. Levashov, A. Matthews. Corros. Sci. 111, 753 (2016). Crossref
11. A.S. Gnedenkov, S.L. Sinebryukhov, V.S. Filonina, N.G. Plekhova, S.V. Gnedenkov. J. Magnes. Alloy. In Press. Crossref
12. G. Barati Darband, M. Aliofkhazraei, P. Hamghalam, N. Valizade. J. Magnes. Alloys. 5, 74 (2017). Crossref
13. M.B. Sedelnikova, E. Komarova, Y. Sharkeev, T. Tolkacheva, V. Sheikin, V. Egorkin, et al. Metals. 8, 238 (2018). Crossref

14. Y. Dekhtyar, M.V. Dvornichenko, A.V. Karlov et al. IFMBE Proc. 25, 245 (2009). Crossref
15. S.A.M. Tofail, J. Bauer. Adv. Mater. 28 (27), 5470 (2016). Crossref
16. I.S. Harding, N. Rashid, K.A. Hing. Biomaterials. 26, 6818 (2005). Crossref
17. B. Gottenbos, H.C. van der Mei, F. Klatter et al. Biomaterials. 24, 2707 (2003). Crossref
18. E.G. Komarova, E.A. Kazantseva, V.S. Ripenko, A.L. Zharin, Y.P. Sharkeev. J. Phys. Conf. Ser. 2064, 012077 (2021). Crossref
19. S. Metwally, U. Stachewicz. Mater. Sci. Eng. C. 104, 109883 (2019). Crossref
20. A.S. Lozhkomoev, E.A. Glazkova, O.V. Bakina, M.I. Lerner, I. Gotman, E.Y. Gutmanas, S.O. Kazantsev, S.G. Psakhie. Nanotechnology. 27, 205603 (2016). Crossref
21. A.S. Lozhkomoev, G. Mikhaylov, V. Turk, B. Turk, O. Vasiljeva. In: Springer Tracts Mech. Eng. Springer, Cham (2020) p. 211. Crossref
22. S.S. Timofeev, A.S. Lozhkomoev, S.O. Kazantsev, I.N. Tikhonova, M.I. Lerner. Russ. J. Phys. Chem. A. 95, 1043 (2021). Crossref
23. M.V. Chaikina, N.V. Bulina, O.B. Vinokurova, I.Yu. Prosanov, D.V. Dudina. Ceram., 45, 16927 (2019).
24. A.L. Zharin. In: Nanosci. Technol. (Ed. by B. Bhushan). Heidelberg, Springer-Verlag (2010) p. 687. Crossref
25. K.U. Pantsialeyeu, A.U. Krautsevich, I.A. Rovba, V.I. Lysenko, R.I. Vorobey, O.K. Gusev, A.L. Zharin. Dev. and Meth. of Meas. 8 (4), 386 (2017). Crossref
26. C. Ma, A. Nagai, Y. Yamazaki, T. Toyama, Y. Tsutsumi, T. Hanawa, W. Wang, K. Yamashita. Acta Biomater. 8, 860 (2012). Crossref
27. D. Zhao, Y. Lu, Z. Wang, X. Zeng, S. Liu, T. Wang. Int. J. Refract. Hard. Met. 54, 417 (2016). Crossref
28. F. Jahanmard, F.M. Dijkmans, A. Majed, H.C. Vogely et al. ACS Biomater. Sci. Eng. 6 (10), 5486 (2020). Crossref
29. S. Liu, J. Zeng. Surf. Coat. Technol. 352, 15 (2018). Crossref
30. W. Yang, B. Jiang, A. Wang, H. Shi. J. Mater. Sci. Technol. 28 (8), 707 (2012). Crossref
31. Yu.P. Sharkeev, K.S. Popova, K.A. Prosolov, E. Freimanis, Yu. Dekhtyar, I.A. Khlusov. J. Surf. Invest. X. Ray. 2, 95 (2020). Crossref